Robotica (2022), **40**, pp. 316–328
doi:10.1017/S0263574721000564

CAMBRIDGE UNIVERSITY PRESS

RESEARCH ARTICLE

Development of a mechanical decoupling surgical scissors for robot-assisted minimally invasive surgery

Xingze Jin[1], Mei Feng[1,*], Zhiwu Han[2], Ji Zhao[3], Hankun Cao[4] and Yaoyuan Zhang[4]

[1]School of Mechanical and Aerospace Engineering, Jilin University, Changchun City, China, [2]College of Biological and Agricultural Engineering, Jilin University, Changchun City, China, [3]School of Mechanical and Automation, Northeastern University, Shenyang City, China and [4]College of Automotive Engineering, Jilin University, Changchun City, China
*Corresponding author. Email: fengmei@jlu.edu.cn

Received: 11 September 2019; **Revised:** 12 April 2021; **Accepted:** 13 April 2021; **First published online:** 31 May 2021

Keywords: surgical instrument, minimally invasive surgery, robot-assisted surgery, surgical robot, mechanical decoupling

Abstract

In minimally invasive surgery, surgical instruments with a wrist joint have better flexibility. However, the bending motion of the wrist joint causes a coupling motion between the end-effector and wrist joint, affecting the accuracy of the movement of the surgical instrument. Aiming at this problem, a new gear train decoupling method is proposed in the paper, which can automatically compensate for the coupled motion in real-time. Based on the performance tests of the instrument prototype, a series of decoupling effects tests are carried out. The test results show that the surgical instrument has excellent decoupling ability and stable performance.

1. Introduction

Robot-assisted minimally invasive surgery (RMIS) has been widely used in thousands of hospitals around the world in recent ten years, bringing millions of patients to advanced surgical treatment. In RMIS, only a few surgical incisions of 0.5∼1.0 cm in length are placed on the patient, and the operation is performed using robotic instruments [1, 2, 3]. Based on absorbing the advantages of minimally invasive surgery, RMIS further reduces the size of surgical incisions, the amount of bleeding, and postoperative recovery time, helping patients recover their bodies faster and better [4, 5, 6, 7, 8, 9]. This is not only due to the real-time high-definition feedback of the image of the surgical area by the imaging system but also due to the precise operation of the robotic instruments by the surgeon [10, 11, 12, 13, 14, 15].

However, it is not comfortable for surgeons to manipulate robotic instruments. This is because the robotic instrument is allowed to pivot about the incision point, rotate about, and translate along its longitudinal axis to prevent the incision from being torn. Therefore, a degree of freedom (DOF) of rotation is added between the end-effector and the shaft of the robotic instrument, such as the da Vinci instruments with EndoWrist technology, a series of robotic instruments designed by Intuitive Surgical for the da Vinci Surgical System [16, 17, 18, 19]. This rotation joint acts like a wrist movement and is called a wrist joint. The addition of the wrist joint greatly improves the flexibility of robotic instruments but also introduces coupling motion between the wrist joint and end-effector. Because of the large aspect ratio of robotic instruments, the tendon-driven method is widely used to achieve power transmission, and the movement of the cords create a coupling motion [20, 21, 22, 23]. The coupling movement of the robotic instrument can seriously affect the operation and result in extremely adverse consequences.

Generally, two methods are accessible, which are software compensation method and mechanical compensation method. Admittedly, the software method that eliminates the coupled motion by compensating an angle calculated by algorithms [24, 25] may have advantages including simpler mechanism and lower assemble cost. The da Vinci Surgical System has been already successfully clinically applied

and commercially available, adopts serialization robotic instruments that adopt software to eliminate coupled motion [26, 27]. However, the defects can cause severe problems, which contain the failure of the software caused by the failure of electronic components. In sharp contrast, the mechanical method is much safer for a mechanism that will never be affected by electronic component faults. Li et al. [28] proposed a robotic instrument with a modularized wrist consisting of four joint units. The traction cords of the wrist joint are evenly distributed along the circumference, and the traction cords of the end-effector pass through the center of the circle. It uses this method of cords distribution to solve the coupling motion. However, since the cord is along a linear path between the joints rather than a circular arc in an ideal state, the bending motion of the wrist joint still produces millimeter order errors in the traction cords of the end-effector. In other words, it has minimized the effects of coupling motion but did not eradicate the coupling motion. This causes a small change in the amount of clamping force or shearing force of the end-effector caused by the coupling motion during the use of the robotic instrument. Hagn et al. [29, 30] designed a surgical robot named MIRO. The instrument of the MIRO has a wrist consisting of a two DOF cable-driven universal joint. The traction cords of the end-effector pass through the hole on the axis of the wrist joint and the long shaft of the instrument in turn. Similarly, although the coupling motion at the wrist joint is greatly weakened, the traction cords still produce a small amount of error. Niu et al.31 proposed a new MIS robot with modular design. It uses a mechanical decoupled method to eliminate the coupled motion between the wrist joint and the forceps, enhance the dexterity of surgical instrument, and improve the independence of each motor. Although the coupled motion is avoided by designing the path of the traction cords of the forceps, the forceps are supported by the shaft of the wrist joint, and the stability may become poor when it is subjected to a large force. A surgical instrument designed by Feng et al. [32] proposed a mechanical method to eliminate the coupled motion of a cable-driven wrist by the use of planetary gear. However, in multiple sets of repeated tests of the robotic instrument, there have been many cases of cords breakage. This may be because the transmission arrangement and cords winding are not reasonable enough. This mechanism, namely planetary gear, can be greatly improved.

In this paper, an oversimplified but novel gears mechanism based on the configuration of robotic instrument with a wrist joint is proposed. By this mean, the coupling motion of the robotic instrument is eliminated, and there is no redundant control difficulty, the independence of the software subsystem is improved and the time required to replace an instrument is shortened. In the following sections, the design of the mechanism is shown, taking surgical scissors as an example. And the conclusions are drawn based on a series of experiments of the instrument.

2. Proposed Surgical Instrument

2.1. Coupling motion analysis

A rigid surgical instrument refers to an instrument that has a relatively solid shaft between the end-effector and driving system. Generally, a rigid surgical instrument driven by cords has three or four DOFs. Considering the flexibility of the instrument, the movement of the wrist and end-effector is independent. However, coupling motion exists between the end-effector and the wrist: a pitching motion of the wrist will cause an undesirable movement of the end-effector, causing much inaccuracy in a practical application.

$$\triangle\alpha = \frac{r_p}{r_s} \times \left(\theta' - \theta\right) \tag{1}$$

$\triangle\alpha$ – the angle of the coupling motion,
rp – radius of pulley A,
rs – radius of scissors axis,
θ – the beginning wrap angle,
θ' – the ending wrap angle.

https://doi.org/10.1017/S0263574721000564 Published online by Cambridge University Press

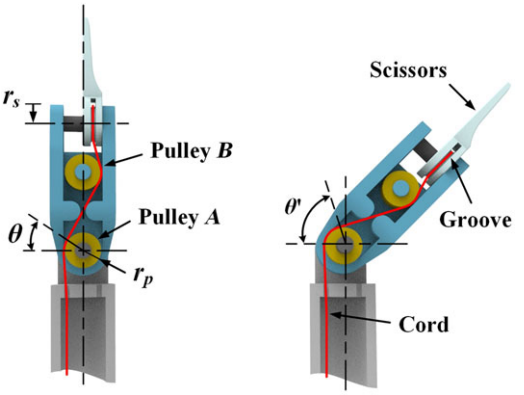

Figure 1. *The coupling motion of the wrist of the surgical instrument.*

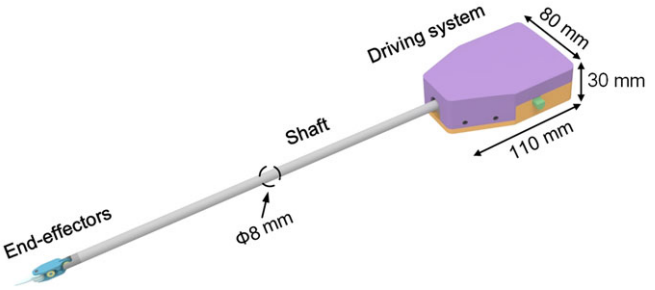

Figure 2. *Surgical instrument.*

Figure 1 shows the principle of the coupling motion. The wrist pivotally installs on the shaft and the end-effector pivotally installs on the wrist. The axis of pulley *A* which the scissors' driven cord wraps around in non-slip mode for accurate transmission is coaxial with the wrist. When the pitching motion – the wrist rotates around its axis – occurs, the wrap angle of the scissors' driven cord on pulley *A* changes from θ to θ' thus causing a change of the cord length around pulley *A*. As a consequence, the scissors rotate synchronously around its axis. The wrap angle can be described by Eq. (1). Different instruments have different r_s and r_p which depend on functions and sizes. So different instruments have different coupling motions.

2.2. Design of the configuration

It is a great requirement to achieve high flexibility and precision under the condition that not only is the diameter of the long shaft, but it requires enough shearing force. To cooperate with a trocar, the diameter of surgical instruments is usually 5, 8, and 10 mm. To take into account the overall strength of the instrument, the diameter of the shaft used in this paper is 8 mm.

The surgical instrument contains three main parts that are the driving system, long shaft, and end-effector. The instrument with the main dimensions is shown in Fig. 2. The driving system uses electric machinery to drive the end-effector, though the long shaft, with steel cords.

And the instrument has four DOFs, shown in Fig. 3 and Table I, which completely implement its functional requirement. The first DOF is the long shaft rotating around the direction of length. The second DOF is the rolling of the wrist. And the other two DOFs are the pitching movement and the opening and closing motion of the scissors.

https://doi.org/10.1017/S0263574721000564 Published online by Cambridge University Press

Table I. *DOFs of surgical instrument and range of motions.*

Shaft rotation	$\omega = \pm 90°$
Wrist rotation	$\theta = \pm 90°$
Scissors pitching	$\eta = 0° \sim 180°$
Scissors opening-closing	$\gamma = 0° \sim 180°$

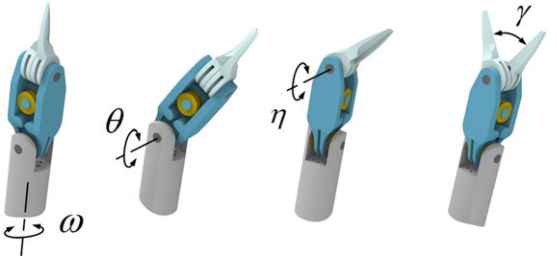

Figure 3. *DOFs of the surgical instrument.*

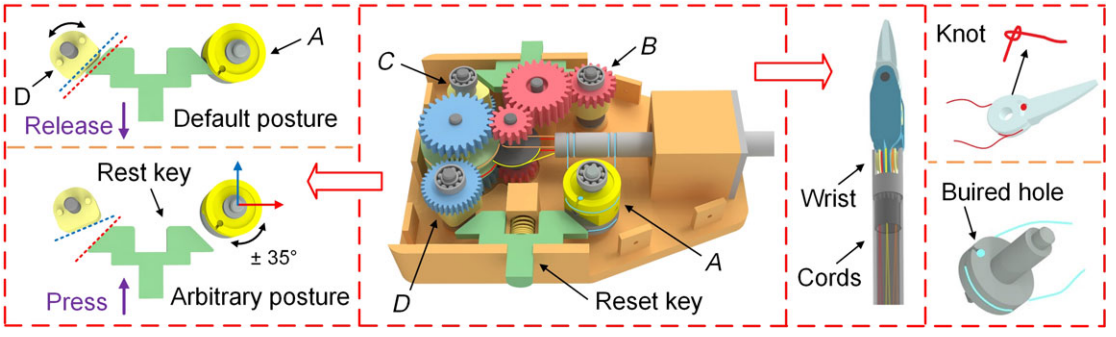

Figure 4. *A schematic diagram of the driving system and the wiring.*

2.3. Design of the driving system

The driving system is shown in Fig. 4. Four driving plates all connect with their electric machinery to transfer the driving force from motors to the long shaft and end-effector. The driving plate *A* drives the shaft to rotate, the driving plate *B* achieves the pitching motion of the wrist, and the driving plates *C* and *D* control the scissors.

Figure 4 also shows the transmission of cords. Combined with the schematic diagram of the transmission system in Fig. 5, the transmission process of the cords is described briefly. For the wrist, the cord, first, is wrapped around pulley *B*, then passes through the inner cavity of the longshaft, and finally wraps around the wrist. The cords wrap around pulley *C* and pulley *D* synchronized with motor *C* and motor *D*. After limited by the pulleys fixed on the wrist, the cords pass through the inner cavity of the long shaft and are fixed with the scissors finally. The cord of the long shaft connects the pulley fixed on the driving plate *A* to the shaft directly.

It is worth pointing out that each of the cords mentioned above wraps around its groove tightly and works in a nonslip mode so that a cord and its driven part can move synchronously and transit accurately. Moreover, to install cords in such a confined space, a subtle structure is proposed. As shown in Fig. 4, there is a hole beside the groove and a knot which is tied in the middle of one cord, dividing the cord into two parts is stuck by the hole. In this way, the joints are connected with the driving pulleys and their movements are synchronized.

https://doi.org/10.1017/S0263574721000564 Published online by Cambridge University Press

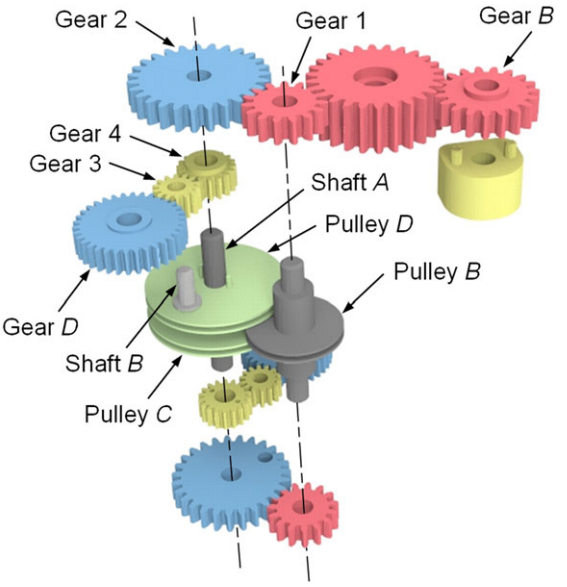

Figure 5. *A schematic diagram of the decoupling module.*

In addition, a pair of reset keys are designed on both sides of the driving system. When the reset key is pressed, the four driving plates of the surgical instrument are quickly restored to the default initial state, which is convenient for the instrument to be quickly installed or removed from the mechanical arm. To realize the rapid reset of the instrument, the pulley of each driving plate is designed as D-type (a plane is cut out on the pulley), and two oblique planes are designed at the top of the reset key. As shown in Fig. 4, the reset key realizes the relative motion with the driving system through a spring. When the reset key is pressed, the spring is compressed. As the reset key gradually approaches the driving plate, the oblique plane at the top of the reset key touches the plane of the pulley and drives the driving plate to rotate until the two planes fit. When the two planes fit together, it is the initial position state of the driving plate. Through the design of the transmission ratio of the pulley and the end-effector, the diameter of the pulley and the end-effector is determined, so that the rotation angle of each pulley is in the range of $\pm 35°$. The simulation results showed that the driving plate can be adjusted to the initial angle by the reset key in this range of motion. When the reset key is released, the pair of reset keys return to their original position under the thrust of the spring.

3. Coupling Compensation Method

3.1. Design of coupling compensation mechanism

It is of great necessity to note that the coupling motion between the wrist and end-effector is unidirectional when applying the configuration of the wrist. As can be seen from Fig. 1, there will be a coupling motion of the end-effector when the wrist is doing pitching movement, while there will be no effect on the wrist when the end-effector moves. In view of this, the authors considered using a gear train to solve the coupling problem. Gear transmission has the advantages of compact structure, high load-carrying capacity, and reliable movement, simultaneously, it can realize synchronous movement and one-way transmission.

The schematic diagram of the uncoupling mechanism is shown in Fig. 5. As can be seen from the transmission box structure diagram, a gear train is assembled between driving plate *B*, driving plate *C*, and the driving plate *D* to connect the three. Gear 3 is fixed on gear 2, and gear 2 can rotate around shaft *A*. Besides, gear 4 is fixed on pulley *D* and they are fixed on shaft *A* together. Figure 6 shows

https://doi.org/10.1017/S0263574721000564 Published online by Cambridge University Press

Table II. *Gearbox parts symbol declaration.*

$\triangle L$ – wrist line length change	θ_B – Wrist movement input
r_B – Gear B index circle radius	θ_{P1} – the angle of rotation of the pulley 1
r_{G1} —– gear 1 index circle radius	θ_{G2} —– the angle of rotation of the gear 2
r_{G2} – gear 2 index circle radius	θ_{P2} —– the angle of rotation of the pulley 2
r_{G3} —– gear 3 index circle radius	r_{G4} – gear 4 index circle radius

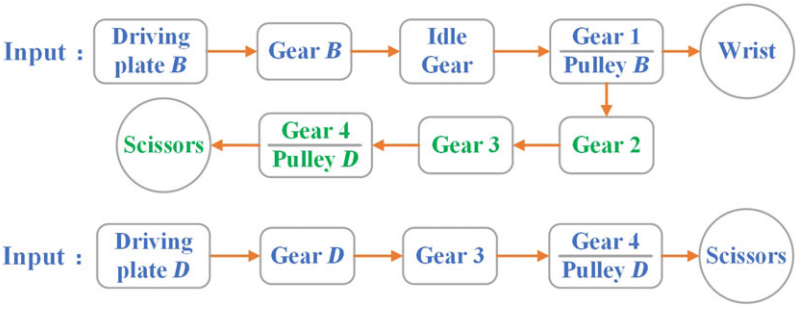

Figure 6. *Flow chart of wrist motion and scissors motion.*

the flow chart of wrist motion and surgical scissors motion. When the motor drives the wrist, gear B rotates, through an idler, passing the force to gear 1 which is fixed with pulley B, so the wrist achieves pitching motion. At the same time, part of the force passes to gear 2. When gear 2 rotates, shaft B rotates around shaft A, while gear D is immovable since it is fixed on the motor. As a consequence, the driving force passes to gear 4 and it drives pulley D to rotate. In this way, the coupling motion of the scissors is compensated. In contrast, when the motor drives the scissors, gear 3 drives gear 4 directly and the force passes to pulley D to drive the scissors. Because the motor is immovable, the force cannot pass to gear 1, and hence the end-effector moves independently without an influence on the wrist. Therefore, the mechanism meets the requirement that achieves a unidirectional compensation between the end-effectors and the wrist. Besides, it is worth pointing out that the wrist moves independently, while the movement of the end-effector is a superposition of its movement and the compensation movement.

With the premise of ensuring functional requirements, this mechanism adopts much fewer gears and has a more compact structure and less error of a gear system. As long as the transmission ratio is designed correctly, the decoupling motion can be realized, so that it can not only ensure the movement in practical application but also simplify the replacing operation.

3.2. Calculation of the transmission ratio

Detailed calculation of the transmission ratio and accurate motion compensation have important significance for the operation accuracy of the surgical instrument. Due to the design of the end-effector, the diameter of the guide wheel of the wrist joint is the same as that of the pulley. Therefore, as long as the linear velocity of the cord that pulls the wrist joint is the same as the line that drives the end-effector, and the direction of the additional motion of the end-effector is opposite to the compensation motion, the coupling motion is compensated. The symbol declaration for each part of the gearbox is shown in Table II.

From the wheel relationship in Fig. 5, we can see that:

$$\Delta L = r_B \cdot \theta_B = r_{G1} \cdot \theta_{P1} = r_{G2} \cdot \theta_{G2} \tag{2}$$

$$r_{G4} \cdot \theta_{G2} = r_{G3} \cdot \theta_{P2} \tag{3}$$

https://doi.org/10.1017/S0263574721000564 Published online by Cambridge University Press

Figure 7. *The prototype of the surgical instrument.*

Figure 8. *Surgical instrument performance tests.*

From Fig. 1 and Eq. (2), we can see that:

$$r_{P2} \cdot \theta_{P2} = r_{P1} \cdot \theta_{P1} \tag{4}$$

From the Eqs. (2), (3), and (4), the following relationship can be obtained:

$$\frac{r_{P1}}{r_{P2}} = \frac{r_{G1}}{r_{G2}} \cdot \frac{r_{G4}}{r_{G3}} \tag{5}$$

The proportional relationship of Eq. (5) is the relationship between the number of teeth between the gears in the decoupling gear train. The size of each transmission component can be determined by the proportional relationship between the diameter of the fixed cord and the diameter of the surgical cord cutter, and referring to the overall size of the transmission case, combined with Eq. (5).

4. Experiments and Results

In order to examine the performance of the proposed surgical instrument, including rotation accuracy of the shaft, bending accuracy of the wrist, as well as decoupling, a prototype is fabricated, and it used the method of tendon-driven to transfer power to the end-effector. The prototype is shown in Fig. 7.

4.1. Surgical instrument performance tests

Rotational motion of the shaft and bending motion of the wrist are used to adjust the posture of the surgical instrument and are the most frequently used by doctors during surgery. To verify the movement accuracy of the instrument, Hexagon's Articulated Arm Three Coordinates Measuring Machine was used for measurement. The experimental process is shown in Fig. 8.

https://doi.org/10.1017/S0263574721000564 Published online by Cambridge University Press

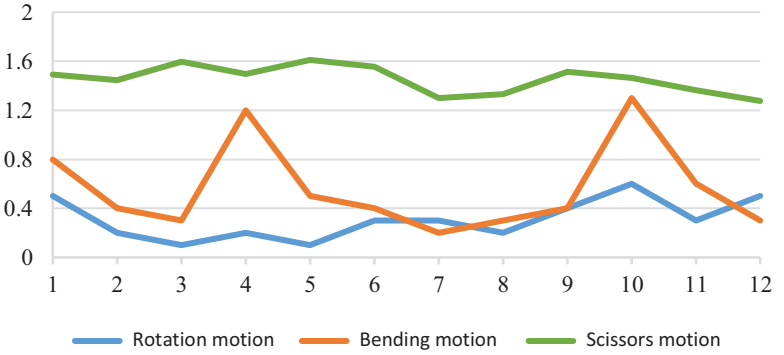

Figure 9. *Tests of motion accuracy of the surgical instrument.*

In the rotational motion test, the initial state of the surgical instrument is recorded as 0°, each time rotated 30°, and rotated 12 times in the same direction for a total of 360°. Measurement was taken after each rotation of the instrument. The rotation error is shown in Fig. 9. It can be seen that the error of each rotation of the instrument is about 0.2°∼0.6°. In the bending motion test, the initial state of the surgical instrument is denoted as 0°, and it is first bent upward, each time bent by 30°, bent to 90°, and then returned downwards to the initial state. In the same way, the instrument bends downward from its initial state and returns. Measurement was taken after each bending of the instrument. The bending error is shown in Fig. 9. It can be seen that the error of each bending of the instrument is about 0.2°∼1.3°. Similarly, the surgical scissors motion accuracy test was also performed. The surgical scissors were closed and their initial state was recorded as 0°. After the test started, the scissors were deflected from the 0° position to one side, each time deflected by 30°, turned to 90° and then deflected to the other side, and finally returned to the 0° position. The pitching error is shown in Fig. 9. It can be seen that the error of each deflection of the instrument is about 1.3° ∼ 1.6°.

4.2. Surgical instrument decoupling test

If the instrument cannot achieve a good decoupling effect, it will certainly cause serious interference to surgery, most likely to have serious operational errors. Therefore, the decoupling effect of the surgical instrument is an important factor to determine whether the instrument can be put into use. To verify the coupling cancellation between the instrument wrist movement and the operation of the surgical scissors, the following verification experiments were conducted. To verify the coupling elimination between the wrist movement of the instrument and the surgical scissors, the following tests were performed.

The marked points *A* and *B* at the edge of the two surgical scissors were selected, and the marked point *C* on the side of the surgical scissors was selected, and the decoupling effect of the surgical instrument was tested by the relative positional change between the three marking points, as shown in Fig. 10. Ideally, when the wrist is rotated, the relative positional relationship between the points *A*, *B*, and *C* is constant. To detect the change of the distance between the three points, the position information of three points is obtained. This group of experiments uses the Aurora series electromagnetic tracking system produced by NDI of Canada. During the test, the wrist joint was repeatedly rotated in the range of −90° to +90°. The position data of the three marked points obtained by the measurement are processed and analyzed. The result is shown in Fig. 11. The distance deviation between the marked points *A* and *B* is between 0 and 2.3 mm, and the distance deviation between the marked points *A* and *C* is between 0 and 1.8 mm, the distance between the marked points *B* and *C* is between 0 and 1.3 mm.

The coupling motion caused by wrist motion may cause a change in the relative position between the marked points, causing a change in the shearing force of the surgical shearing. It is also possible to cause the overall deflection of the two blades, at which point two points on the blade the relative position

https://doi.org/10.1017/S0263574721000564 Published online by Cambridge University Press

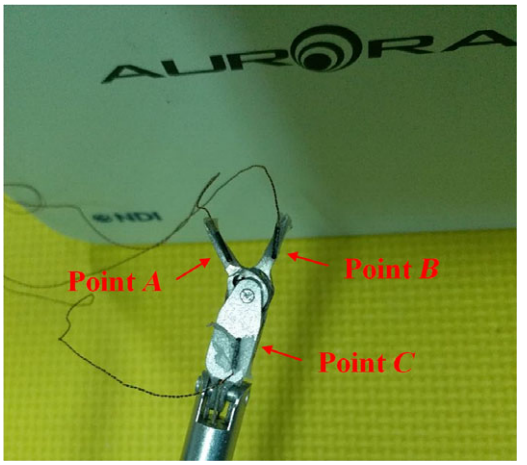

Figure 10. *Set marking points on the surgical scissors.*

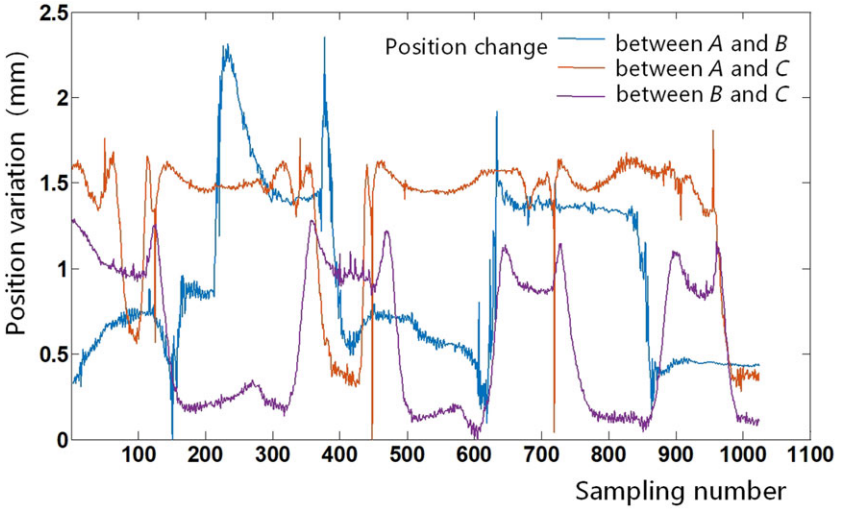

Figure 11. *Change in position between marked points.*

between the two does not change, the shearing force of the scissors does not change, but the point of application of the surgical scissors is offset. To study the effect of the latter case on the operation of surgical instruments, this section conducted further testing studies.

As shown in Fig. 12, the positional relationship between the three marked points in the coupled motion is depicted. In the picture, P_A, P_B with P_C indicates the initial position of points A, B, and C, $P_A^{'}$, $P_B^{'}$ with $P_C^{'}$ for the position of the points A, B, and C after the movement of the wrist, the point O is the center of rotation of the two blades. Known from the structure of the instrument and the movement of the wrist joint, P_C with $P_C^{'}$ the two points coincide and the position of the O point does not change. Also in Fig. 12, OP_A with OP_B the length is 15 mm; P_AP_B is the initial distance between points A and B, $P_A^{'}P_B^{'}$ is the distance between the marked points A and B during the rotation of the wrist joint; OP_A with OP_B the angle between θ represents the initial angle between the blades, $OP_A^{'}$ with $OP_B^{'}$ angle between $\theta^{'}$ represents the angle between the blades during the rotation of the wrist. P_CP_A versus $P_CP_A^{'}$ the angle

https://doi.org/10.1017/S0263574721000564 Published online by Cambridge University Press

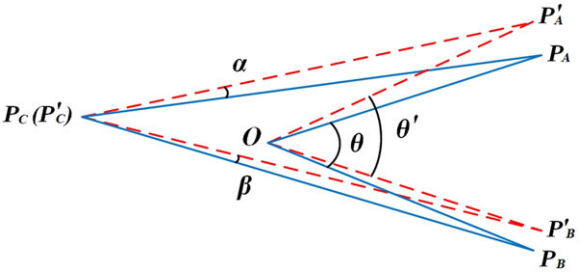

Figure 12. *Angle deviation of the surgical scissors.*

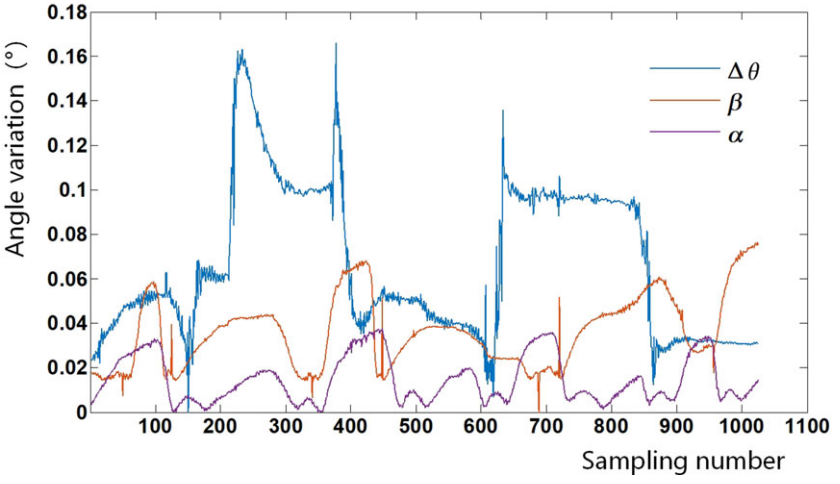

Figure 13. *Angle variation curve.*

between α,$P_C P_B$ versus $P_C P_B^{'}$ the angle between β reflects the rotational deviation between the blade and the wrist joint.

Obtained from the above geometric relationship θ function relation:

$$\theta = 2 * \arcsin \frac{P_A P_B}{2OP_A} \tag{6}$$

When the wrist is rotated, θ with $\theta^{'}$ the difference between the reflections reflects the change in angle between the blades:

$$\Delta\theta = 2 * \left(\left| \arcsin \frac{P_A P_B}{2OP_A} - \arcsin \frac{P'_A P'_B}{2OP_A} \right| \right) \tag{7}$$

α and β can be obtained by the following equation:

$$\alpha = \arccos \frac{P_C P_A^2 + P_C P'^2_A - P_A P'^2_A}{2 \cdot P_C P_A \cdot P_C P'_A} \tag{8}$$

$$\beta = \arccos \frac{P_C P_B^2 + P_C P'^2_B - P_B P'^2_B}{2 \cdot P_C P_B \cdot P_C P'_B} \tag{9}$$

After experimental testing, the change of the angle of the surgical clip is obtained, as shown in Fig. 13. As can be seen from the angle change curve, α the maximum value is 0.04°, β the maximum value

https://doi.org/10.1017/S0263574721000564 Published online by Cambridge University Press

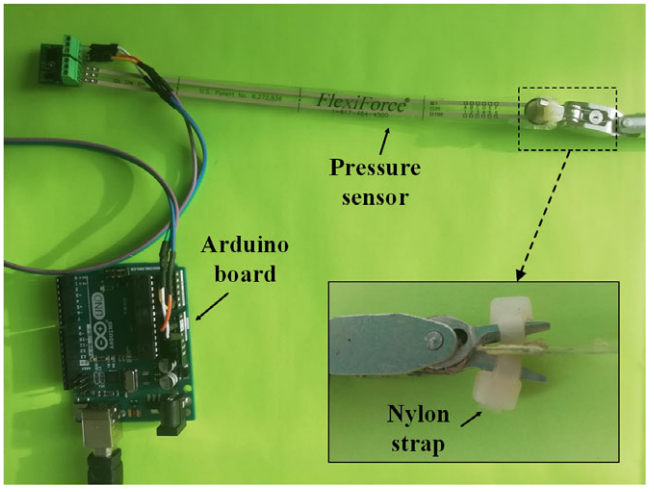

Figure 14. *Shear force fluctuation experiment.*

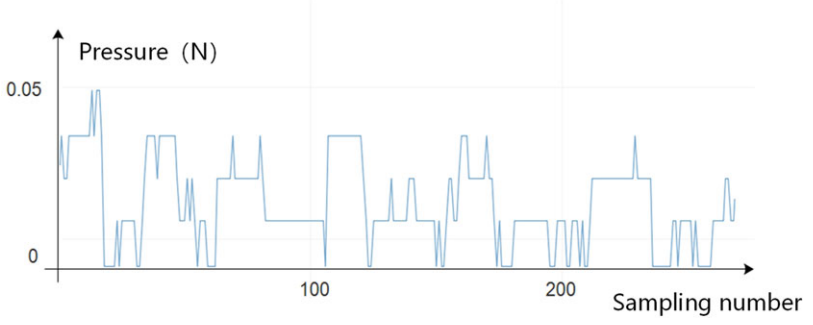

Figure 15. *Shear force fluctuation curve.*

is 0.07°. $\triangle\theta$ can be used to describe the relative attitude change between the blades with a maximum value of 0.17°.

For further verification, by $\triangle\theta$ another test was performed on whether the resulting pressure fluctuations affected the operation of the surgical scissors. The test uses a pressure sensor to measure pressure fluctuations between the two blades during wrist movement. To obtain a sufficient contact area of the pressure sensor and prevent the sensor from being damaged by the blade, a nylon belt is respectively fixed on the two blades. The test process is shown in Fig. 14. During the test, the wrist joint rotates between −90° and +90°. The pressure fluctuation during the test is shown in Fig. 15. It can be seen that the shear pressure fluctuation caused by the coupling error is less than 0.05 N.

It can be seen from the abovementioned plurality of test results that the change of the blade rotation caused by the coupling motion caused by the wrist joint and the change of the cutting force between the blades are very small, and the influence on the operation of the surgical instrument is negligible. It also proves the effectiveness of the decoupling method proposed in this paper, and the rigid surgical instrument is designed to meet the surgical operation requirements.

5. Conclusion

The surgical instrument is the actuator of the MIS system and is the part that contacts directly with the patient. It can be said that the performance of surgical instruments is related to the quality of surgery. To improve the flexibility of the surgical instrument, a rotating joint similar to the human wrist is added at

https://doi.org/10.1017/S0263574721000564 Published online by Cambridge University Press

the end of the instrument, and a coupled motion is also introduced between the end-effector and the wrist joint. Therefore, whether it can well eliminate the coupling of the instrument is an important indicator of whether the instrument is easy to use. In this paper, the authors designed a RMIS surgical instrument with mechanical decoupling. The decoupling mechanism adopted a new gear train decoupling method to realize the synchronization of coupling motion and compensating motion of the instrument, thus achieving the goal of real-time automatic compensation of coupling motion. This decoupling method has high stability and reliability and also ensures the concision of the end-effector of the instrument. To verify the performance of the instrument, a series of tests were performed on the prototype. And it showed high rotation accuracy and wrist bending accuracy. Most importantly, the surgical instrument demonstrated excellent decoupling capability. Future work will be focused on the optimization of the surgical instrument, including the improvement of the motion accuracy (optimizing the layout of the guide wheels and the tension state of the traction cords, etc.) and mechanical properties, as well as preclinic experiments of the surgical instrument.

Acknowledgments. The authors thank the surgeons and medical stuff of Jilin University First Hospital for their supports. This work was supported by the National Natural Science Foundation of China (Grant No. 51975241); the Natural Science Foundation supported by the Science and Technology Department of Jilin Province (Grant No. 20180101076JC); the Key R&D Project supported by the Science and Technology Department of Jilin Province (Grant No. 20200404150YY); and the Jilin Province Industrial Technology Research and Development Project (Grant No. 2019C048-3).

Conflicts of Interest. The authors report no conflicts of interest. The authors alone are responsible for the content and writing of the paper.

References

[1] G. B. Cadiere, J. Himpens, O. Germay, R. Izizaw, M. Degueldre, J. Vandromme, E. Capelluto and J. Bruyns, "Feasibility of robotic laparoscopic surgery: 146 cases World," *J. Surg.* **25**(11), 1467–1477 (2001).

[2] A. R. Lanfranco, A. E. Castellanos, J. P. Desai and W. C. Meyers, "Robotic surgery: A current perspective," *Ann. Surg.* **239**(1), 14–21 (2004).

[3] C. Simillis, V. A. Constantinides, P. P. Tekkis, A. Darzi, R. Lovegrove, L. Jiao and A. Antoniou, "Laparoscopic versus open hepatic resections for benign and malignant neoplasms–a meta-analysis," *Surgery* **141**(2), 203–211 (2007).

[4] H. W. Donias, H. L. Karamanoukian, G. D"Ancona and E. L. Hoover, "Minimally invasive mitral valve surgery: From Port Access to fully robotic-assisted surgery," *Angiology* **54**(1), 93–101 (2003).

[5] M. Menon, A. Tewari, J. O. Peabody, A. Shrivastava, S. Kaul, A. Bhandari and A. K. Hemal, "Vattikuti Institute prostatectomy, a technique of robotic radical prostatectomy for management of localized carcinoma of the prostate: Experience of over 1100 cases," *Urol. Clin. North Am.* **31**(4), 701–717 (2004).

[6] K. K. Badani, S. Kaul and M. Menon, "Evolution of robotic radical prostatectomy: Assessment after 2766 procedures," *Cancer* **110**(9), 1951–1958 (2007).

[7] M. C. Bell, J. Torgerson, U. Seshadri-Kreaden, A. W. Suttle and S. Hunt, "Comparison of outcomes and cost for endometrial cancer staging via traditional laparotomy, standard laparoscopy and robotic techniques," *Gynecol. Oncol.* **111**(3), 407–411 (2008).

[8] G. P. Haber, S. Crouzet and I. S. Gill, "Laparoscopic and robotic assisted radical cystectomy for bladder cancer: A critical analysis," *Eur. Urol.* **54**(1), 54–62 (2008).

[9] B. M. Benway, S. B. Bhayani, C. G. Rogers, L. M. Dulabon, M. N. Patel, M. Lipkin, A. J. Wang and M. D. Stifelman, "Robot assisted partial nephrectomy versus laparoscopic partial nephrectomy for renal tumors: A multi-institutional analysis of perioperative outcomes," *J. Urol.* **182**(3), 866–872 (2009).

[10] G. Dogangil, B. L. Davies and F. Rodriguez y Baena, "A review of medical robotics for minimally invasive soft tissue surgery," *Proc. Inst. Mech. Eng. H* **224**(5), 653–679 (2010).

[11] L. P. Aitchison, C. K. Cui, A. Arnold, E. Nesbitt-Hawes and J. Abbott, "The ergonomics of laparoscopic surgery: A quantitative study of the time and motion of laparoscopic surgeons in live surgical environments," *Surg. Endoscopy* **30**(11), 1–9 (2017).

[12] S. Takazawa, T. Ishimaru, K. Harada, K. Deie and A. Hinoki, "Evaluation of surgical devices using an artificial pediatric thoracic model: A comparison between robot-assisted thoracoscopic suturing versus conventional video-assisted thoracoscopic suturing," *J. Laparoendoscopic Adv. Surg. Tech. Part A* **28**(5), 622–627 (2018).

[13] C. A. Nelson, M. A. Laribi and S. Zeghloul, "Multi-robot system optimization based on redundant serial spherical mechanism for robotic minimally invasive surgery," *Robotica* **37**(7), 1202–1213 (2018).

[14] R. Rana, P. Gaur, V. Agarwal and H. Parthasarathy, "Tremor estimation and removal in robot-assisted surgery using lie groups and EKF," *Robotica* **37**(11), 1904–1921 (2019).
[15] A. Torabi, M. Khadem, K. Zareinia, G. R. Sutherland and M. Tavakoli, "Using a redundant user interface in teleoperated surgical systems for task performance enhancement," *Robotica* **38**(10), 1880–1894 (2020).
[16] J. Binder, R. Bräutigam, D. Jonas and W. Bentas, "Robotic surgery in urology: Fact or fantasy?," *BJU Int.* **94**(8), 1183–1187 (2004).
[17] N. G. Hockstein, J. P. Nolan, B. W. O'Malley Jr and Y. J. Woo, "Robotic microlaryngeal surgery: A technical feasibility study using the daVinci surgical robot and an airway mannequin," *Laryngoscope* **115**(5), 780–785 (2005).
[18] J. M. Smith, H. Stein, A. M. Engel, S. McDonough and L. Lonneman, "Totally endoscopic mitral valve repair using a robotic-controlled atrial retractor," *Ann. Thorac. Surg.* **84**(2), 633–637 (2007).
[19] R. Hompes, S. M. Rauh, M. E. Hagen and N. J. Mortensen, "Preclinical cadaveric study of transanal endoscopic da Vinci(R) surgery," *Br. J. Surg.* **99**(8), 1144–1148 (2012).
[20] A. J. Madhani, G. Niemeyer and J. Kenneth Salisbury Jr, "The Black Falcon: A Teleoperated Surgical Instrument for Minimally Invasive Surgery," *1998 IEEE/RSJ International Conference on Intelligent Robots and Systems, 1998. Proceedings* (1998).
[21] K. Harada, K. Tsubouchi, M. G. Fujie and T. Chiba, "Micro Manipulators for Intrauterine Fetal Surgery in an Open MRI," *IEEE International Conference on Robotics & Automation* (2005).
[22] H. Luo, J. Ding and S. Wang, "A Master-Slave Robot System for Minimally Invasive Laryngeal Surgery," *IEEE International Conference on Robotics & Biomimetics* (2009).
[23] C. He, S. Wang, Y. Xing and X. Wang, "Kinematics analysis of the coupled tendon-driven robot based on the product-of-exponentials formula," *Mech. Mach. Theory 60(none),* 90–111 (2013).
[24] Z. Cao, Q. Xiao, R. Huang and M. Zhou, "Robust neuro-optimal control of underactuated snake robots with experience replay," *IEEE Trans. Neural Netw. Learn. Syst.* **29**(1), 208–217 (2018).
[25] X. Ma, C. Song, P. W. Chiu and Z. Li, "Autonomous flexible endoscope for minimally invasive surgery with enhanced safety," *IEEE Rob. Autom. Lett.* **4**(3), 2607–2613 (2019).
[26] J. Tierney Michael, T. Cooper, C. Julian, J. Blumenkranz Stephen, S. Guthart Gary and G. Younge Robert, Surgical robotic tools, data architecture, and use (2001).
[27] D. P. Noonan, G. P. Mylonas, A. Darzi and G. Z. Yang, "Gaze Contingent Articulated Robot Control for Robot Assisted Minimally Invasive Surgery," *IEEE/RSJ International Conference on Intelligent Robots & Systems* (2008).
[28] K. Li, B. Pan, F. Zhang, W. Gao, Y. Fu and S. Wang, "A novel 4-DOF surgical instrument with modular joints and 6-Axis Force sensing capability," *Int. J. Med. Rob.* **13**(1) (2017).
[29] U. Hagn, R. Konietschke, A. Tobergte, M. Nickl, S. Jorg, B. Kubler, G. Passig, M. Groger, F. Frohlich, U. Seibold, L. Le-Tien, A. Albu-Schaffer, A. Nothhelfer, F. Hacker, M. Grebenstein and G. Hirzinger, "DLR MiroSurge: A versatile system for research in endoscopic telesurgery," *Int. J. Comput. Assist. Radiol. Surg.* **5**(2), 183–193 (2010).
[30] S. Thielmann, U. Seibold, R. Haslinger, G. Passig and G. Hirzinger, "MICA - A New Generation of Versatile Instruments in Robotic Surgery," *IROS 2010, IEEE International Conference on Intelligent Robots and Systems* (2010).
[31] G. Niu, B. Pan, F. Zhang, H. Feng, W. Gao and Y. Fu, "Dimensional synthesis and concept design of a novel minimally invasive surgical robot," *Robotica* **36**(5), 715–737 (2018).
[32] F. Mei, F. Yili, P. Bo and Z. Xudong, "An improved surgical instrument without coupled motions that can be used in robotic-assisted minimally invasive surgery," *Proc. Inst. Mech. Eng. H* **226**(8), 623–630 (2012).

Cite this article: X. Jin, M. Feng, Z. Han, J. Zhao, H. Cao and Y. Zhang (2022). "Development of a mechanical decoupling surgical scissors for robot-assisted minimally invasive surgery", Robotica **40**, 316–328. https://doi.org/10.1017/S0263574721000564